A European endeavor for optimizing Zonal Isolation, Drilling and Exploitation of EGS projects

REPORT AND RESULTS OF ETHZ-INVOLVED SUB-TASKS (2.1, 3.1, 3.2, 3.4, 4.2, 4.3)

Authors: Xiang-Zhao Kong and Martin O. Saar (ETHZ)

Date: January 2022

The GEOTHERMICA is supported by the European Union's HORIZON 2020 programme for research, technological development and demonstration under grant agreement No 731117

ZoDrEx

Contents

Figures

1. Introduction

This report presents the borehole characterization work at the Bedretto Underground Laboratory for Geosciences and Geoenergies (BULGG) and the flow-through experiments at the GREAT Visualization Lab of the Geothermal Energy and Geofluids Group (GEG) at ETH Zurich (ETHZ). ETHZ was involved in the borehole characterization in WP 2 (Demonstration of wellbore segmenting technologies), seismic risk and monitoring, data analysis and modelling, and demonstration of simulation with different zone isolation systems in WP 3 (Demonstration of reservoir simulation technologies and lifting optimization), and sampling and analysis of effluents from plant in WP 4. However, the involvement of ETH Zurich in WP 4 was minimized due to the suspending of collaboration between ETHZ, GES, ESG in WP 4. This deviation has been approved by Swiss Bundesamt für Energie (BFE).

2. Methodology

2.1 Field campaign at BULGG

For the field campaign at the BULGG, ETHZ used the Acoustic Televiewer (ATV) and Optical Televiewer (OTV) to log the boreholes (Figure 1). ETHZ analysed the stress state at the BULGG by using mini-frac tests, and dry (packer) reopening tests. The fracture closure pressure was analysed with several techniques, including G-function, square root of time, bilinear pressure-decay, and jacking pressure. ETHZ performed the step-rate injection tests to determine the fracture and matrix injectivity in the BUL. ETHZ conducted analyses of the dilatometer test to obtain the modulus of deformation and modulus of elasticity of the in-situ rock mass in the BUL. Using the ATV and caliper logs, ETH Zurich conducted borehole breakout analysis. ETHZ also contributed to the design and construction of the sensors (Streamer 2.0) of the seismic monitoring network in the BULGG.

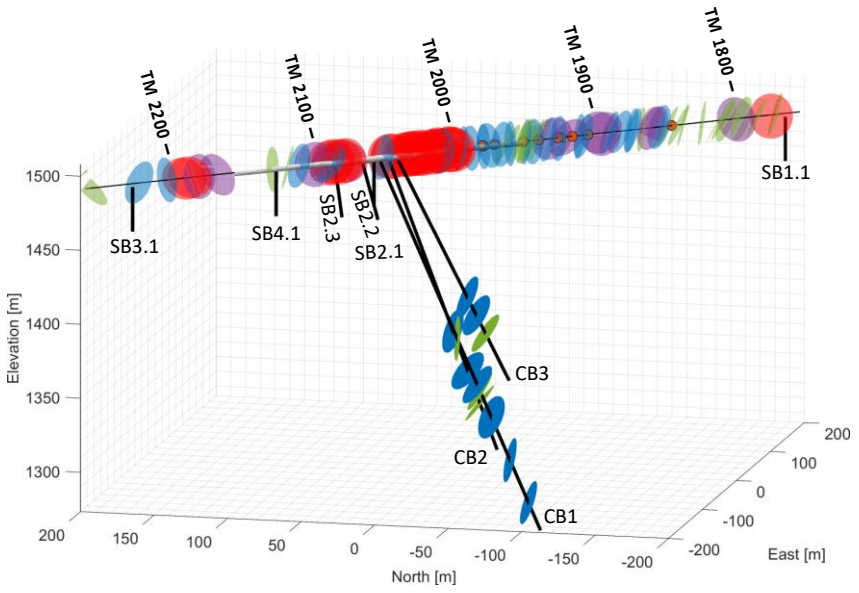

Figure 1. All ETHZ works in WP 2 used boreholes in the BULGG. Analyses of borehole fractures and stress were done with Boreholes SB1.1, SB2.2 and SB3.1, and breakout analysis (additional work) was done with Boreholes CB1 and CB2.

2.2 Laboratory activities at the GEG Great Visualization Lab

At the GEG Group lab, ETHZ has conducted a series of flow-through experiments. These experiments were conducted using the novel (hydrothermal) flow-through (reactor) system (Figure 2), which employs syringe pumps (up to 100 MPa and a volume of 300 ml) to provide constant fluid flow rates (from 10^{-4} ml/min to 73 ml/min) through core samples located in a dual-end- access triaxial cell. Syringe pumps also maintain outlet pore pressure (i.e., back pressure) and core (pore-fluid) confinement pressure. At the same time, electric band heaters precisely control temperature (up to 200°C) of this triaxial cell. Pressure transducers, installed at the inlet and outlet of the flow-through cell, continuously monitor the differential pressure. To identify the mineral compositions of the rock samples, ETHZ performed Energy Dispersive X-Ray Analysis (EDX) and Scanning Electron Microscope (SEM) analyses. To image the rock pore/fracture geometry, ETHZ performed X-ray Computed Tomography (XRCT) scanning of rock samples (Figure 3). To obtain water chemistry (major ion concentrations) of the effluents, ETH Zurich conducted Inductively Coupled Plasma-mass-spectrometry (ICPMS) measurements.

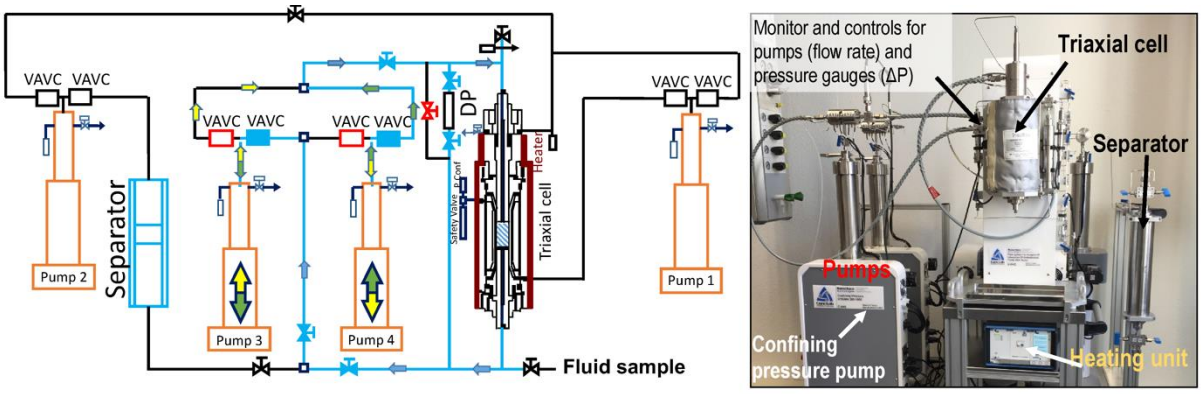

Figure 2. (Right) Reactive flow-through system (reactor) for investigations of chemical and physical processes that affect pore-scale geometries in (fractured) rocks over a wide range of temperatures and (pore-fluid) pressures. (Left) Schematic of our novel flow flow-through system that allows automatic switching between injection pump and back- pressure pump (Pumps 3 and 4) without changing the flow direction.

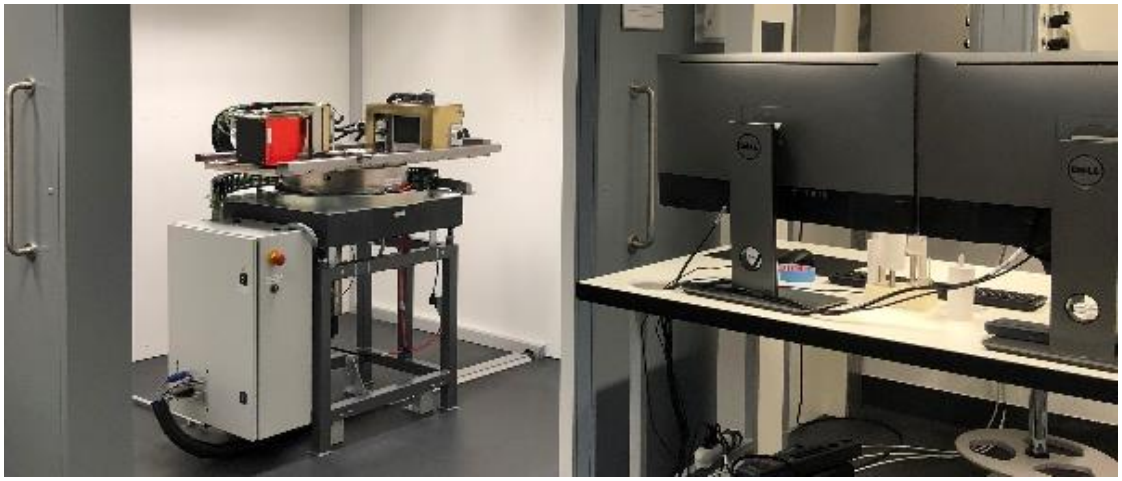

Figure 3. The X-ray Computed Tomography scanner used for rock sample scanning at the GEG Group.

3. Results

3.1 Borehole analyses

ETHZ has completed the proposed work in borehole characterization of WP 2: Zonal isolation. Because of the suspending of collaboration between ETH, GES, and ESG in WP 4 (see explanation on WP 4), ETH Zurich used part of the personnel hours in WP4 to conduct additional work in WP 2. This deviation has been approved by the Swiss Bundesamt für Energie (BFE). In summary, ETHZ has worked on fracture analysis, stress analysis, injectivity test, measurements of deformation modulus and elasticity modulus, and breakout analysis in WP 2. Here, the work of breakout analysis belongs to the additional work. All works in WP 2 used boreholes in the BULGG. Analyses of borehole fractures and stress were done with Boreholes SB1.1, SB2.2 and SB3.1, and breakout analysis (additional work) was done with Boreholes CB1 and CB2 (Figure 1).

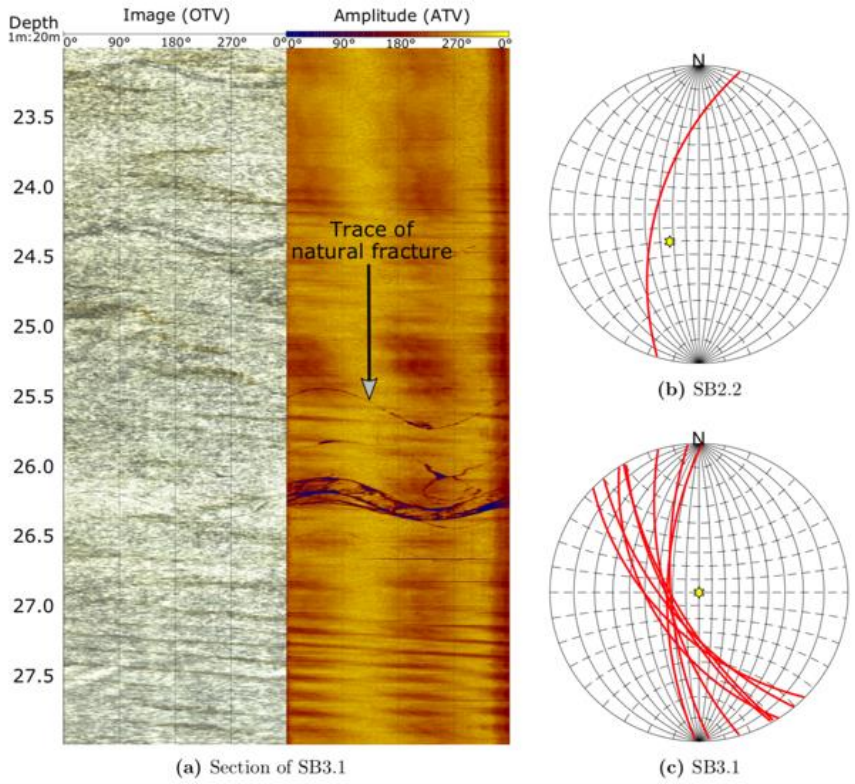

Figure 4. (a) Borehole logging data, ATV and OTV, showing a section with several natural fractures at a depth between 25.5 to 26.5 m in SB.3.1. (b) + (c) Lower hemisphere stereonet with fracture planes of logged natural fractures. The yellow star symbolises the borehole axis. (Bröker, 2019)

Natural and/or induced fractures were identified using the logging images from Boreholes SB2.2 and SB3.1 with the Acoustic Televiewer (ATV) and Optical Televiewer (OTV) (Bröker, 2019). Borehole SB2.2 shows just a single fracture at a depth of 15 m. The fracture dips into a westward direction. More fractures are visible in Borehole SB3.1, but they are limited to a depth of 25 to 27 m and a single fracture at a depth of 29 m. The dip directions vary between W and SW, with strikes between 135 ° to 196 °. Dip angles of fractures in Borehole SB3.1 lie between 54 ° and 71 ° (Figure 4).

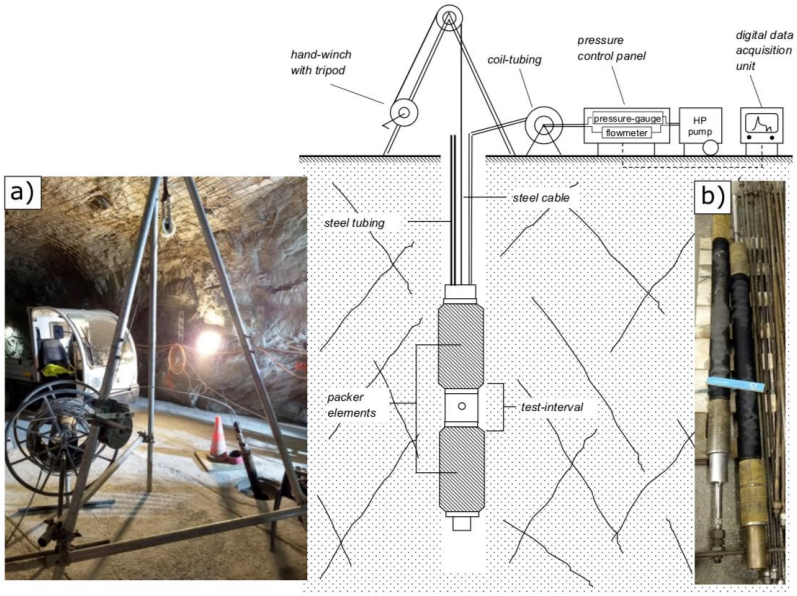

205

206 *Figure 5. Schematic drawing of the mini-frac equipment and set up (by G. Klee, MeSy-Solexperts*
207 *GmbH). Inserted are two pictures from the test site: (a) Tripod, hand-driven winch and coil-tubing;*
208 *packer can be seen inside the borehole; (b) Straddle packer elements (left) and steel tubing (right).*
209 *(Bröker, 2019)*

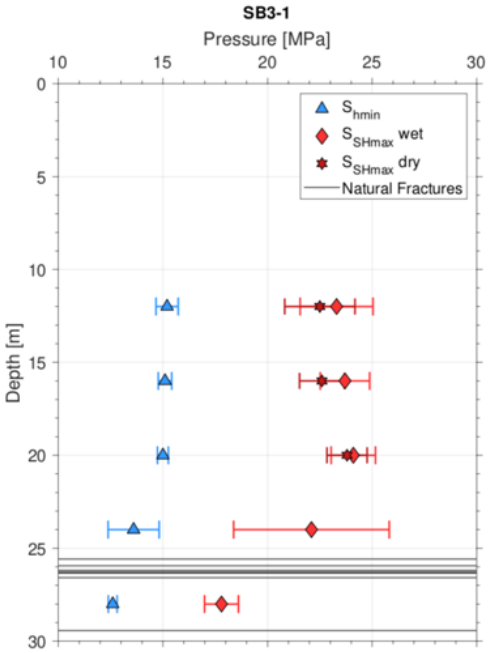

210

211 *Figure 6. The computed minimum (S_{hmin}) and maximum (S_{Hmax}) horizontal stresses at five depth*
212 *intervals in the vertical borehole SB3.1. S_{hmin} is obtained from the fracture closure pressure picked by*
213 *the compliance method, errors are given by the standard deviation per interval. S_{Hmax} is calculated from*
214 *breakdown, reopening, pore pressure and S_{hmin} itself. Grey lines show where natural fractures intersect*
215 *the borehole. (Bröker, 2019)*

The stress state at the BUL was estimated with mini-frac tests and dry (packer) reopening tests (Figure 5). The stresses were measured primarily based on the classic hydraulic fracturing technique, called a mini-frac test. In total, the mini-frac tests were performed in three SB boreholes (i.e., SB1.1, SB2.1, and SB3.1) at five depth intervals. If the instantaneous shut-in pressures in the mini-frac tests are used to derive the magnitude of S_{hmin}, the values of S_{hmin} falls within the range of 13-16 MPa, which is close to the stress magnitude bounded by the friction equilibrium (S_{hmin} ~ 15.3 MPa) with a granite density of 2.7 g/cm^3 and a frictional coefficient (μ) of 0.6 (Figure 6). In each borehole, we performed at least one over-night (typically 12-15 hours) shut-in test to measure the formation pore pressure. Several such shut-in tests indicate that pore fluid pressure (Pp) is between 3 and 6 MPa at the depths of the stress measurements. The estimation of S_{Hmax} can be derived from the difference between the breakdown pressure ($P_{breakdown}$) and the re-opening pressure (Pre-opening), e.g., $S_{Hmax} = 3S_{hmin} - P_{re\text{-}opening} - Pp$. Based on such a relationship, the estimation is that S_{Hmax} is about 0.8~1 of Sv, indicating a normal faulting and/or strike-slip stress environment. If the slip tendencies of both boreholes are summarized using a Mohr circle diagram, compared to the N-S oriented fractures, the NW-SE oriented fractures exhibit higher slip tendency, which can be explained by their orientation relative to the input direction of the minimum horizontal stress.

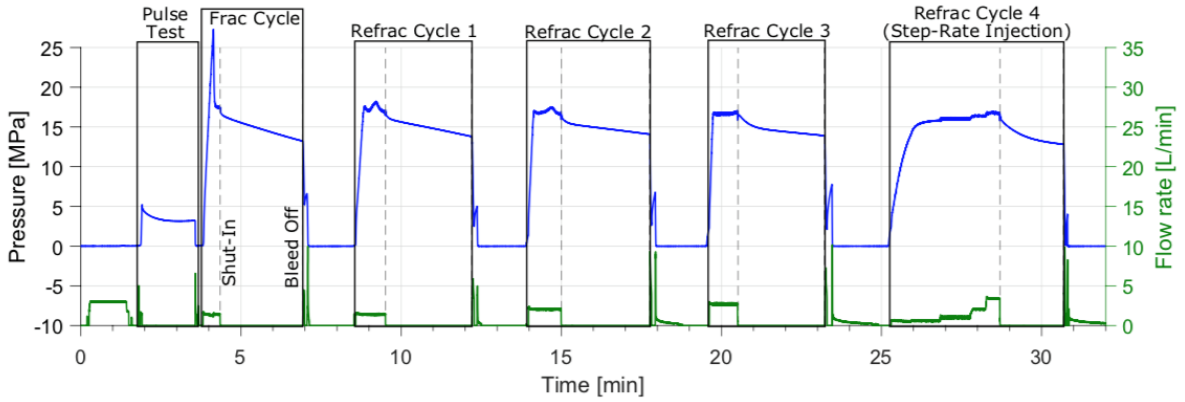

Figure 7. Injection protocol of the mini-frac tests, consisting of an initial pulse test, the fracking/breakdown cycle and four reopening cycles, where the last one is a step-rate injection test. The blue curve shows the pressure inside the interval and the green one the injection flow rate. Black boxes mark the time windows, where fluid is injected into the interval and the pressure transient measured after pumping stopped (dashed line). The shown data are from SB3.1 at 12 m depth. (Bröker, 2019)

To increase the accuracy of fracture reopening pressure measurements and estimate the stiffness of the rock mass, dry (packer) reopening tests were conducted. The technique is based on the so-called sleeve fracturing method. Inside a borehole, a packer is inflated and pressure onto the borehole wall exerted via its membrane. By increasing the pressure further, formation breakdown can be measured, similar to hydraulic fracturing (Figure 8). Consecutive cycles can be used to assess the fracture reopening pressure (Figure 9). The tests can be used to determine the minimum and maximum horizontal stresses in laboratory tests and vertical wells. The fracture closure pressure was analysed with several techniques, including G-function, square root of time, bilinear pressure-decay, and jacking pressure. In most cases, the applied techniques give consistent results within an uncertainty range of 1 to 2 MPa. The fracture compliance method was used to identify the point, where the stiffness of the fracture increases, related to the beginning of its closure. Increasing fracture stiffness

was correlated to a linear or bilinear flow regime on log-log scale plots of the pressure derivative. Formation breakdown, fracture reopening and instantaneous shut-in pressures were picked and compared as well. The results show that intra- and inter-borehole variations and the proximity to naturally fractured regions seem to influence the data quality and pressure values. Natural fractures, identified from on the ATV and OTV borehole logs, are expected to be reactivated in the pressure range reached during the mini-frac tests. As the induced tensile fracture propagates further away from the borehole with every injection cycle, it becomes more and more likely that it intersects pre-existing fractures. This can be seen as multiple closure signature on several of the used diagnostic plots, where it is beneficial to have extended observation times (≥ 1 h) to fully characterise the different closure behaviours.

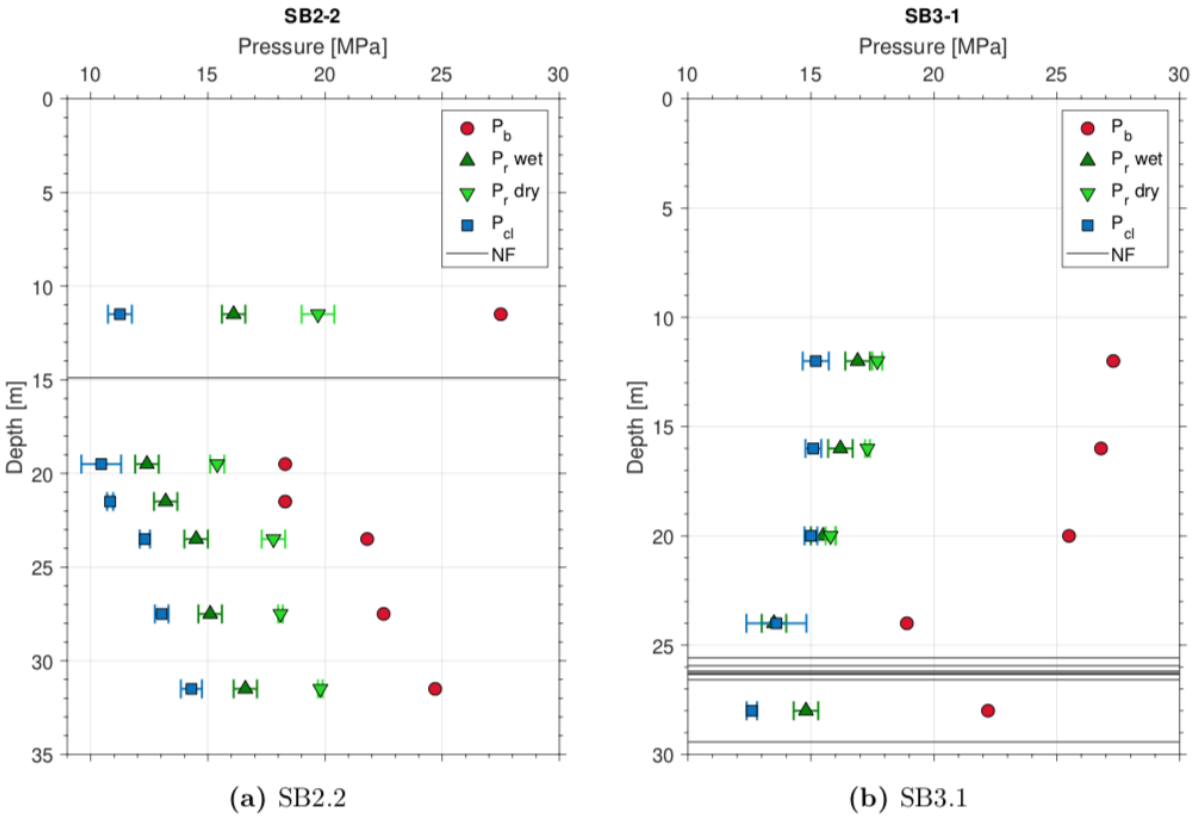

Figure 8. Results for the formation breakdown, fracture reopening and closure pressure along the two boreholes. The estimated errors are given by the standard deviation or are assumed. Traces of natural fractures (NF) are shown as well. Note that the dry reopening tests were not successful in all intervals. P_{cl} is the fracture closure pressure. P_b is the formation breakdown pressure. P_r is the fracture reopening pressure. (Bröker, 2019)

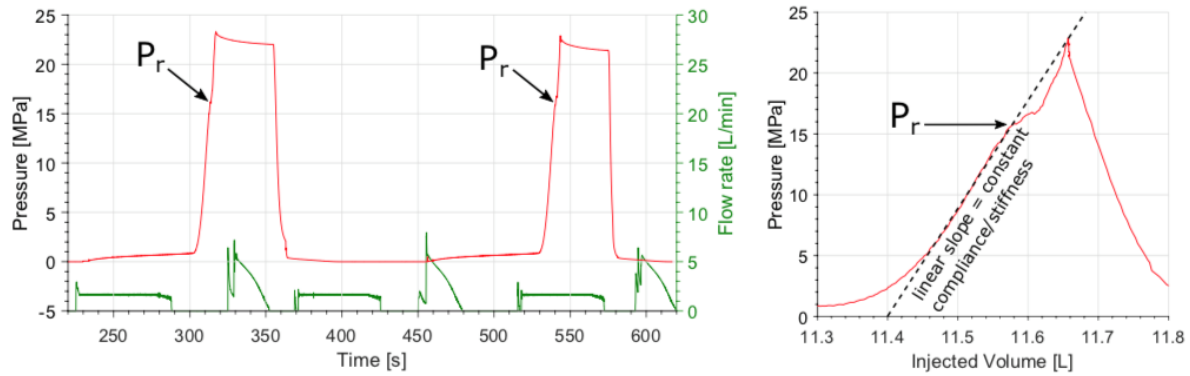

Figure 9. Dry reopening test in SB3.1 at 20m depth. In both plots, the deviation from a linear trend, or kink in the record, showing a decrease in the system stiffness, is taken as the fracture reopening pressure. (Left) Plot of pressure vs. time for the second and third dry reopening cycles. (Right) Plot of pressure vs. injected volume for the third cycle. (Bröker, 2019)

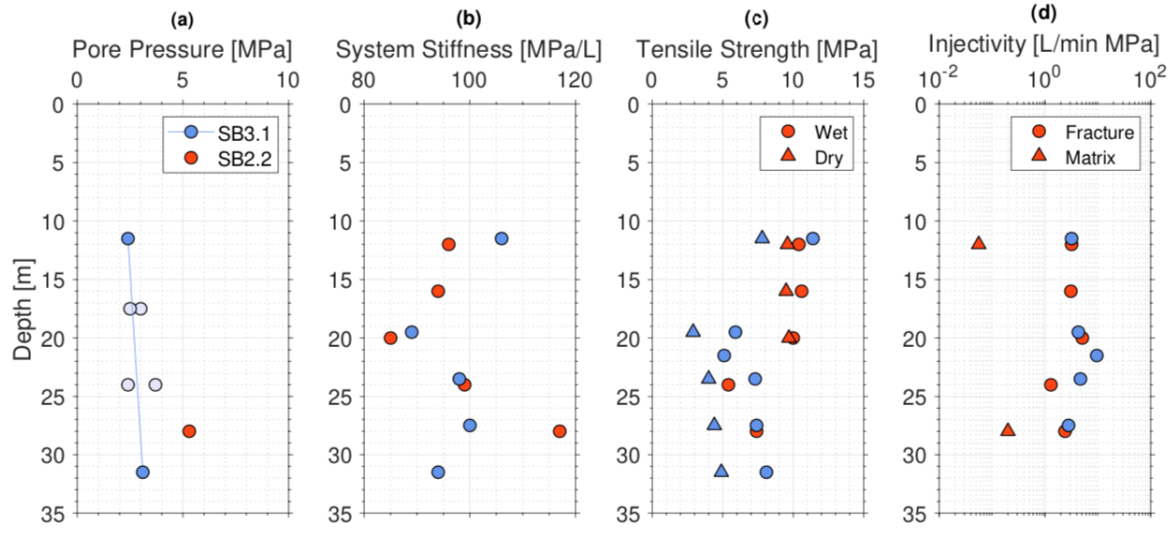

Figure 10. (a) Pore pressure evaluated from extended overnight shut-ins. (b) System stiffness calculated from dry reopening tests. (c) Hydraulic tensile strength calculated from formation breakdown and wet or dry reopening pressures. (d) Injectivity of fracture and matrix estimated from step-rate injection tests. (Bröker, 2019)

The fracture and matrix injectivity were estimated using the step-rate injection tests (Figure 10). Matrix injectivity could just be determined in two intervals in the SB3.1 borehole, due to insufficient data points that indicate pressure versus flow rate. Both injectivity values are on the same order of magnitude with 0.06 and 0.20 L/(min MPa). The fracture injectivity was estimated for all step-rate tests, the average value in SB2.2 borehole is 3.7 L/(min MPa) and in SB3.1 borehole is 3.0 L/(min MPa).

The slip tendencies of both boreholes are summarised in a Mohr circle diagram in Figure 11. Fractures close to the failure line are critically stressed and a fluid injection shifts the Mohr circle and fracture planes, plotted as poles, closer to the failure line. The higher slip tendency of fractures oriented NW-

SE compared to N-S oriented fractures can be explained by their orientation relative to the input direction of the minimum horizontal stress.

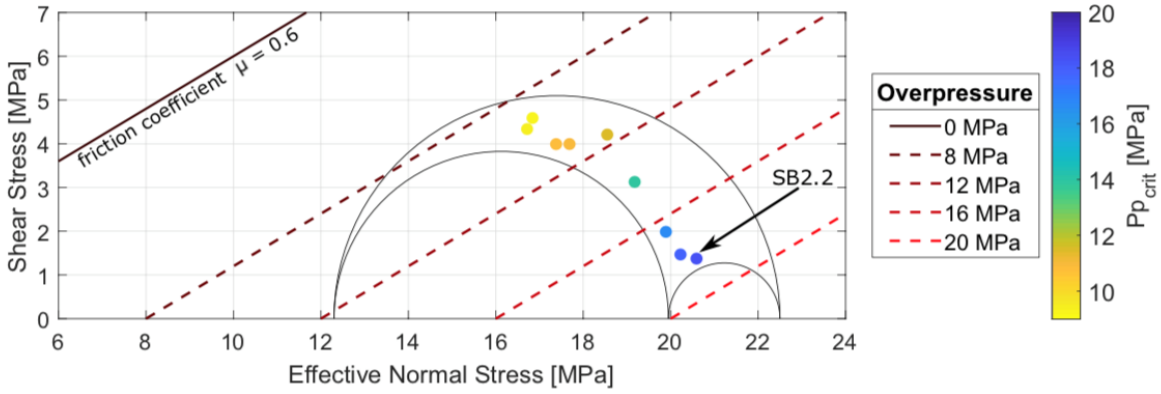

Figure 11. Visualization of the identified natural fractures in a Mohr circle. The fracture planes are colored according to the critical pore pressure increase needed to induce slip. The single fracture occurring in borehole SB2.2 is marked, the other fractures are from SB3.1. The solid line gives the Mohr-Coulomb criteria for fault reactivation. Dashed lines show the failure criterion after an increase in pore pressure through fluid injection, which reduces the effective stress and possibly reactivates optimally oriented faults. (Bröker, 2019)

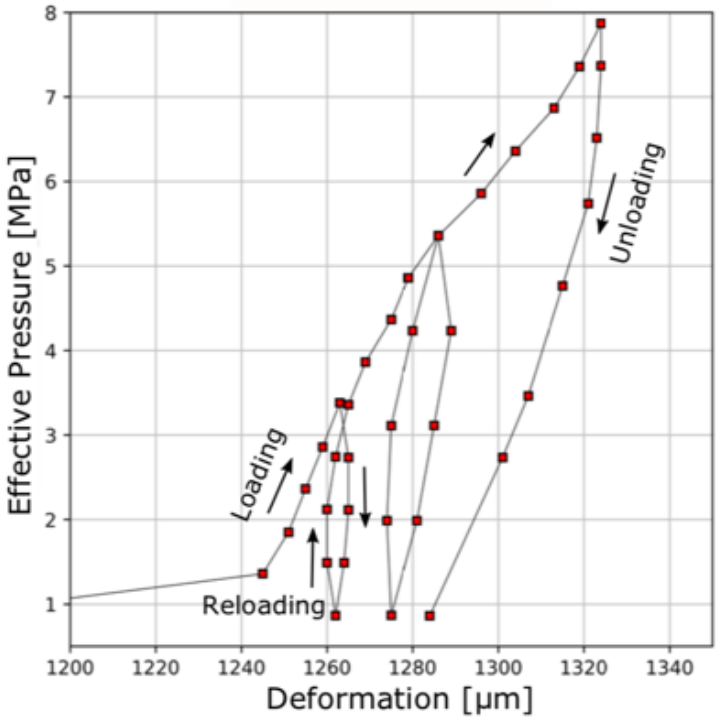

Figure 12. Record from the dilatometer test at 9 m depth in SB2.2 (Bröker, 2019). Shown is the average deformation of the top, middle and bottom displacement transducer. The rising maximum pressure can be seen in all three loading cycles.

The dilatometer test is used to obtain the modulus of deformation and modulus of elasticity of the in-situ rock mass. The tests were conducted at a depth of 9 m in Borehole SB2.2 and 22 m in Borehole SB4.1. The averaged deformation observed from the three transducers during the dilatometer test in SB2.2 can be seen in Figure 12. The first cycle pressurized the rock up to 3.4 MPa, the second one up to 5.4 MPa and the final one up to 7.9 MPa. The average elastic modulus is, also considering the dilatometer test in the vertical borehole SB4.1, 42 MPa ± 18 MPa. The overall average of the deformation modulus from the loading cycle is 12 MPa ± 4 MPa and from the reloading cycle 45 MPa ± 25 MPa. The high standard deviation shows the large scatter of the values.

ETHZ has conducted additional work in WP 2 on in situ stress analysis and borehole breakout analysis. The additional work is covered by part of the personnel hours of WP 4, due to the suspending of collaboration between ETH, GES, ESG in WP 4 (see explanation in WP 4). In these additional works, an azimuth log, tilt log, and caliper log were collected from the ATV logs of Boreholes CB1 and CB2. Breakouts along the boreholes CB1 and CB2 were identified based on the ATV logs: 262 breakouts were identified in CB1 between 120-220 m; 136 breakouts were identified in CB2 between 120-220 m (Figure 13). Discussions were made on variations in breakout presence, orientation and shape, and the underlying processes that cause these variations. Intersections between natural fractures and Boreholes CB 1 and CB 2 were identified using ATV logs and OTV logs. The direct link between borehole orientation, borehole tilt, and breakout presence is investigated, as well as the influence of the rate of change of the orientation and tilt. Estimations were made on the rock strength in areas with breakout presence.

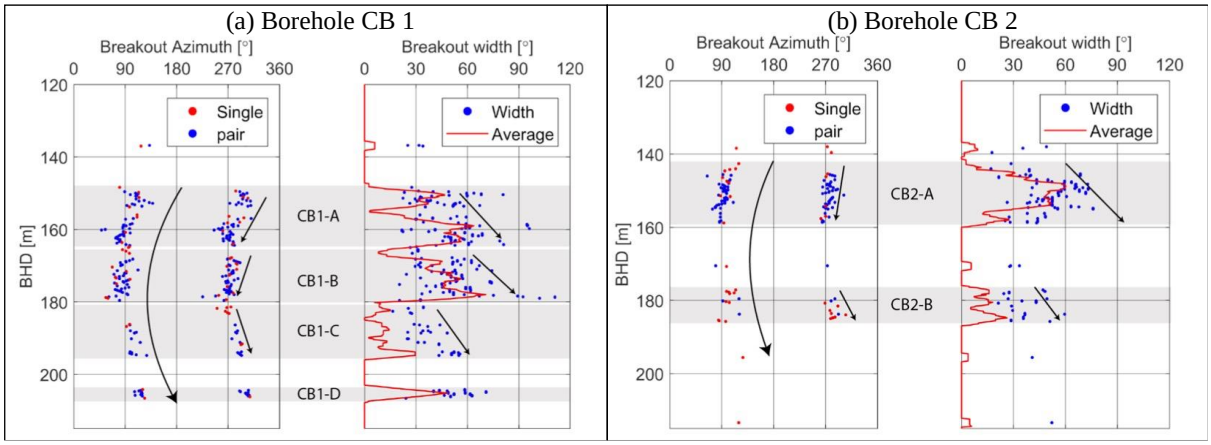

Figure 13. Breakout azimuth and width for Boreholes CB 1 and CB 2, zoomed into interval between 120–220m BHD. Single breakouts and breakout pairs are indicated. Azimuth trend over the complete borehole is indicated, as well as trends in azimuth and width for groups of breakouts identified, CB1A–D and CB2A–B for CB1 and CB2 respectively. Breakout azimuth is given with respect to top of borehole (HS), orientation with respect to magnetic North (NM). (After Limborgh (2020))

3.2 Flow-through experiments and seismic risk analysis at BULGG

In WP 3: Stimulation and production optimization, ETH Zurich has conducted, fracture permeability characterization, mud cake formation, seismic risk analysis, and shear and acidizing stimulation. Similar to WP 2, due to the suspending of collaboration between ETH, GES, ESG in WP 4, the work of shear and acidizing stimulation used another part of the personnel hours. This deviation has also been approved by the Swiss Bundesamt für Energie (BFE).

A series of the transmissivity tests has been conducted on naturally fractured Granodiorite specimens with a diameter of 2.8 cm and a length of 3.5 cm. The composition of the granodiorite specimens was determined, using Energy Dispersive X-Ray Analysis (EDX), to be: quartz, feldspar, biotite and chlorite. For each transmissivity measurement, a constant flow rate was set and the differential pressure (ΔP) between the inlet and the outlet of the specimen was recorded. Later, the confining pressure ($P_{confining}$) and the fluid pore pressure (P_{pore}) were varied to establish different aperture configurations. Finally, the evolution of the hydraulic aperture was mapped under different effective stresses ($P_{confining} - P_{pore}$) (Figure 14). These transmissivity results can be used to elucidate how fracture injectivity will be changed under different effective stresses.

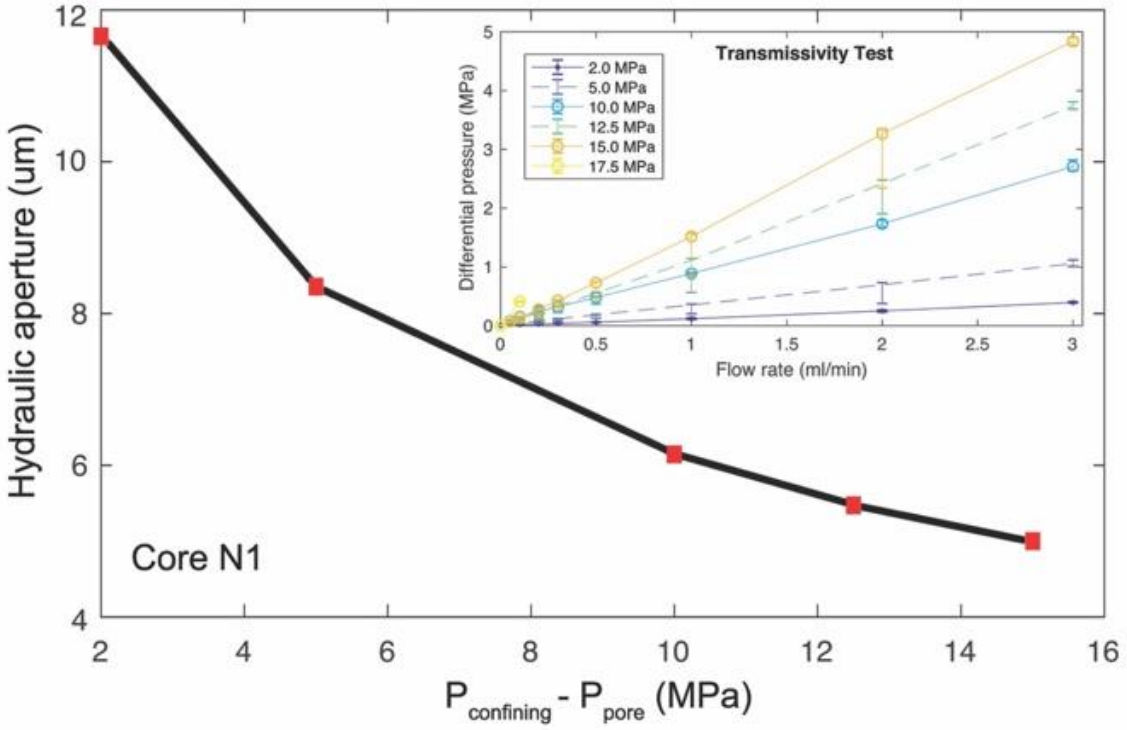

Figure 14. Hydraulic aperture evolution under different effective stresses ($P_{confining} - P_{pore}$).

Fracture permeability is influenced by not only its effective stress, but also shear displacements. To examine how the permeability of fractured granite changes, when subjected to shearing events, induced by hydraulic stimulation, shear experiments were conducted to measure the permeability of granite samples with a single parallel natural/saw-cut fracture (Li et al., 2021). During the experiments. the shear slips were induced by increasing fluid pressure. For all examined specimens, the fracture permeability changes up to one order of magnitude after experiencing shear slips. No

consistent increasing or decreasing trend of permeability evolution was observed, neither for a single slip event, nor for the entire experiment. For most of the specimens, permeability increased during the first few shear slip events, reaching a maximum permeability after a critical shear displacement was achieved (0.0445 mm for Specimen N03, 0.0570 mm for Specimen N21, 0.0715 mm for Specimen N27, and 0.0310 mm for Specimen A28), exhibiting a positive relationship with respect to fracture roughness. Generally, permeability then decreased with further slip events after a large, in most cases the largest, shear displacement.

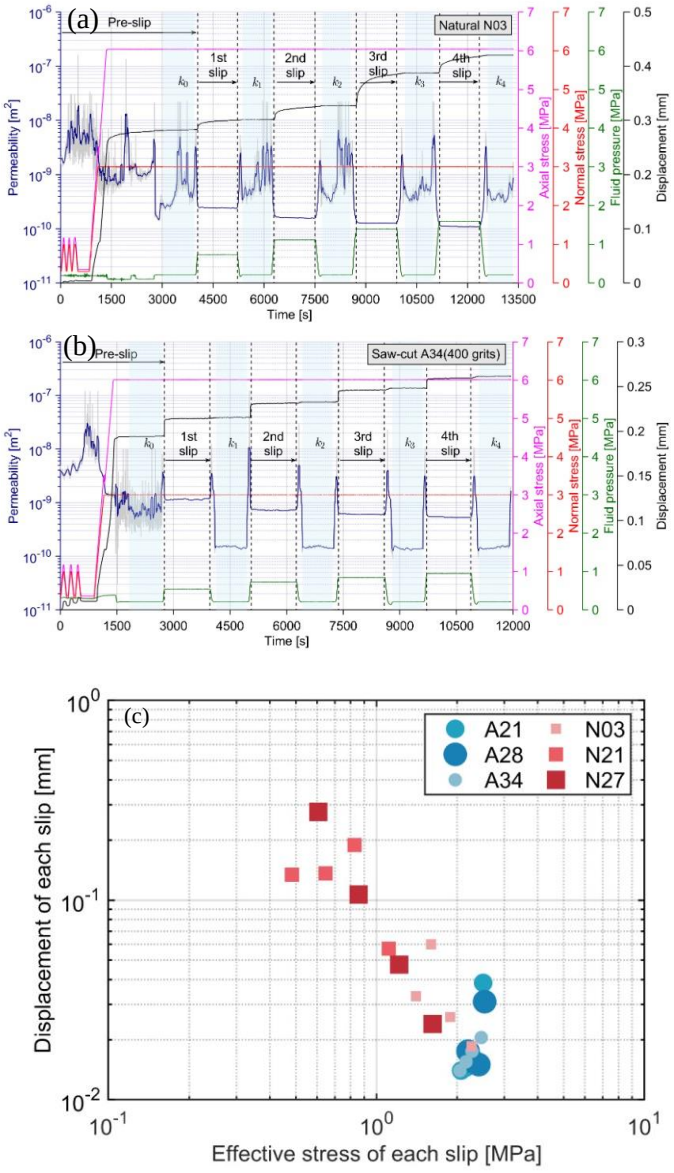

Figure 15. Loading path, accumulated displacement (since the start of the experiment), and calculated permeability (original data in gray and filtered data in dark blue) of Specimens: (a) N03 and (b) A34. The range of shear displacements are marked by dotted lines. (c) Relationship between effective stress and shear displacement for each slip distance on a log-log plot. Specimens with larger fracture roughness values are marked by bigger markers. Specimens N03, N21 and N27 are natural fractures of different modes, and specimens A21, A28 and A34 are saw-cut fractures of different polishing finishes. (After Li et al. (2021))

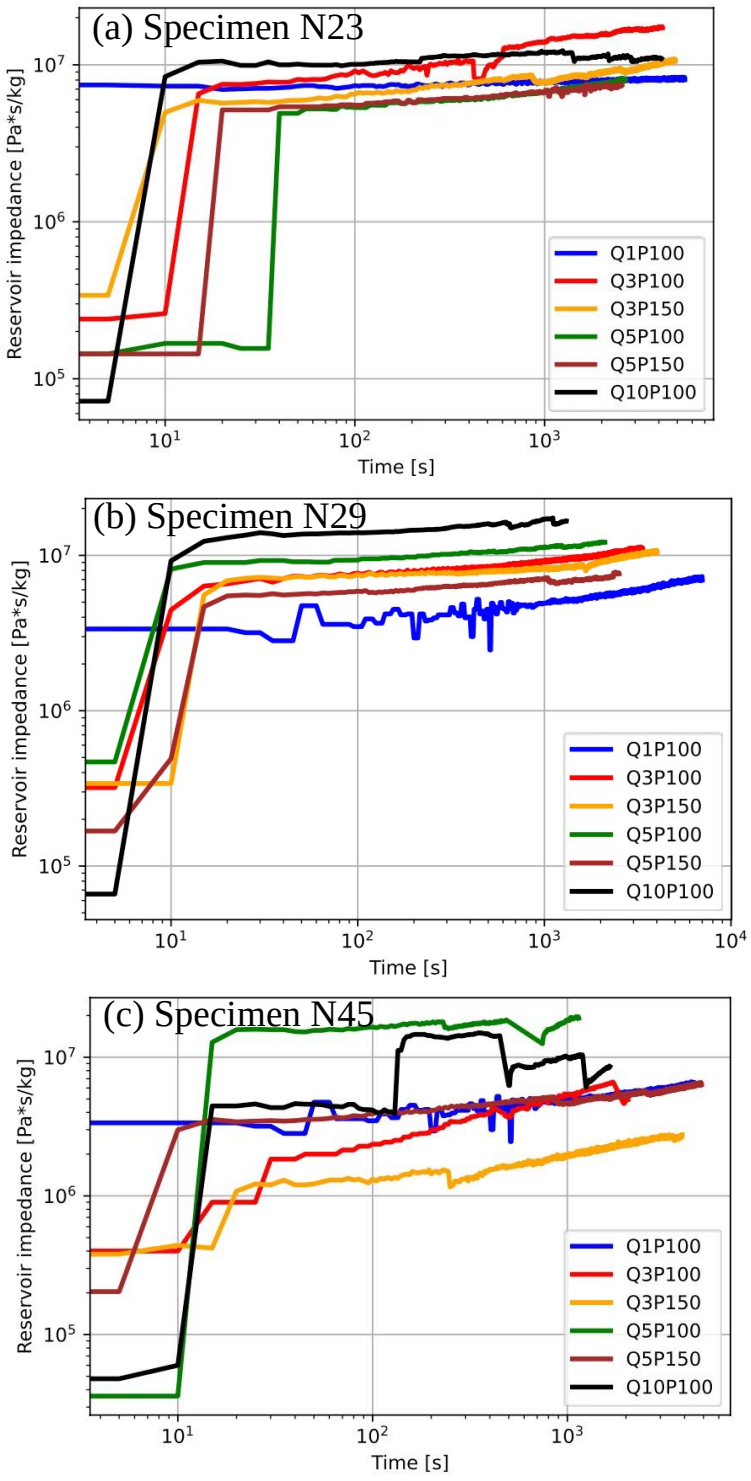

Figure 16. Reservoir impedances for Specimens (a) N23, (b) N29, and (c) N45 during the formation of mud cake. In the legends, the numbers after Q indicate the flow rates with a unit of ml/min, and the numbers after P indicate the back pressures with a unit of bar during the experiment. (After Wang (2021))

Mud cake often forms around wells when drilling mud infiltrates into the permeable zones. Mud cake provides a barrier to prevent further penetration and loss of drilling fluid, as well as a loss of produced fluids, into a permeable formation. It is thus necessary to quantitatively explore the associated phenomena when mud cake is formed within a fracture in a laboratory environment. ETH Zurich conducted a series of laboratory experiments focusing on mud cake formation on the fractures coupled with hydraulic and mechanical processes. Mud cake formation was monitored under reservoir conditions (2 kilometers). The potential effect of mud cake on the hydraulic properties of natural fractures was examined under pressure conditions (downstream pressure of 10 MPa, 15 MPa, and confining pressure of 40 MPa). Three specimens of naturally fractured granodiorite cores from the Grimsel Test Site in Switzerland were subjected to flow-through experiments at room temperature (23°C), due to the unexpected failure of the heating system. Fractures have been imaged using X-ray CT to characterize their surface roughness. Fracture transmissivities have been measured on various pore fluid pressures and effective stresses. Mud has been prepared with calcite ($CaCO_3$) particles of size around 60 micros. In total, 18 experiments have been conducted (Figure 16). Hydraulic aperture and reservoir impedance of fractures were evaluated during the formation of mud cake. In general, the higher injection rate, the higher the amount of mud being brought into the fractures, yielding larger reservoir impedance (Figure 16).

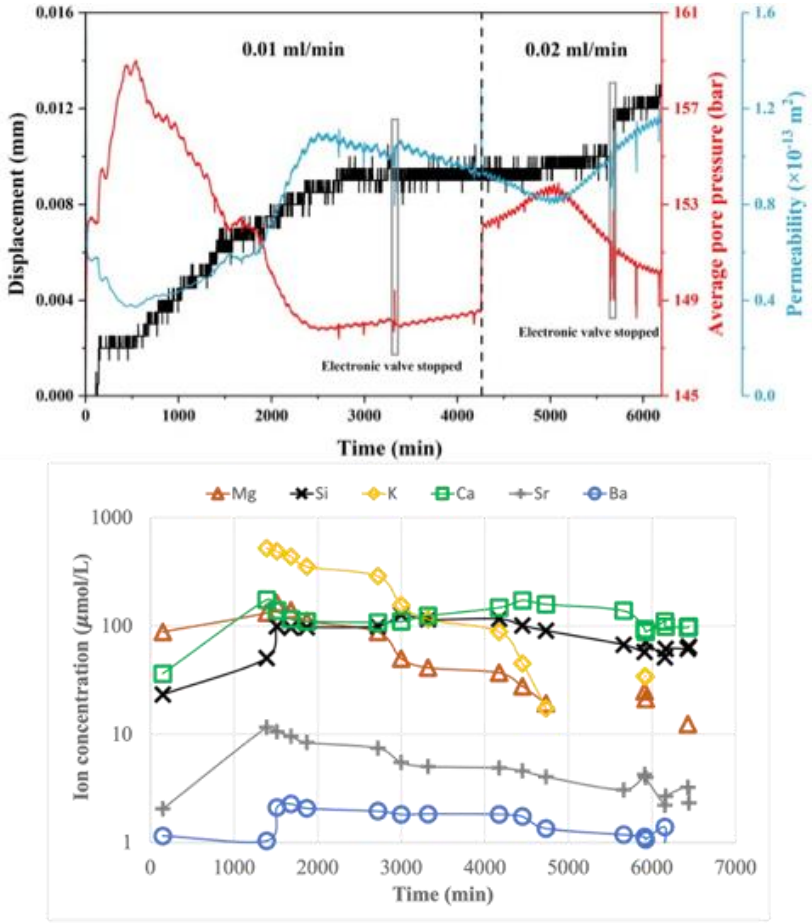

Figure 17. (Top) Shear displacements, average pore fluid pressure, and fracture permeability during the experiment. (Bottom) Major and tracer element concentrations during the experiment. Injection rate was kept at 0.01 ml/min till t=4200 min, and then increased to 0.02 ml/min for the rest of the experiment. (Kong et al., (2021))

When fractures are critically stressed, acidizing stimulation could cause shear slip of fractures. ETH Zurich conducted additional work on shear and acidizing simulation on carbonate-filled fractures. A cylindrical specimen of 2.54 cm in diameter and 3.33 cm in length was sub-cored from a granite sample at a depth of 1897 m in Borehole EPS1 in Soultz, France. SEM analysis indicated that the filling minerals in the fracture are carbonates (mainly $CaCO_3$), quartz and hematite. The specimen was imaged before and after the shear and acidizing simulation using the customised X-ray CT at the GEG Group (Figure 3). Before the shear and acidizing simulation, fracture permeability was measured to be ~10^{-13} m^2 at a normal confinement of 28.5 MPa, a back pressure of 14.5 MPa, and a temperature of 100 ° C. Injection of 1.66 mol/L NaCl brine with 0.001 mol/L HCl was carried out for ~6500 min, under a normal confinement of 28.5 MPa, a back pressure of 14.5 MPa, and a temperature of 100 ° C. Shear displacement of the fracture was continuously monitored with a gauge meter: a total of 12 micrometer displacement was observed during the 6500 min experiment (Figure 17). Effluents from the flow-thought experiment were collected and analyzed using ICPMS to obtain the ion concentrations for geochemical analysis (Kong et al., 2021). Gouge materials from the experiments have been collected and analysed. Using the monitored shear displacements, the combined rigidity of the fracture was estimated to be about 3.29 GPa, the seismic moment magnitude was calculated as 6.9 Nm, the standard seismic moment was determined as 60.8 Nm, and the maximum seismic moments of the two continuous slip events (during injection rate of 0.01 ml/min and 0.02 ml/min) can be computed as 18.61 Nm and 4.96 Nm, respectively (Kong et al., 2021).

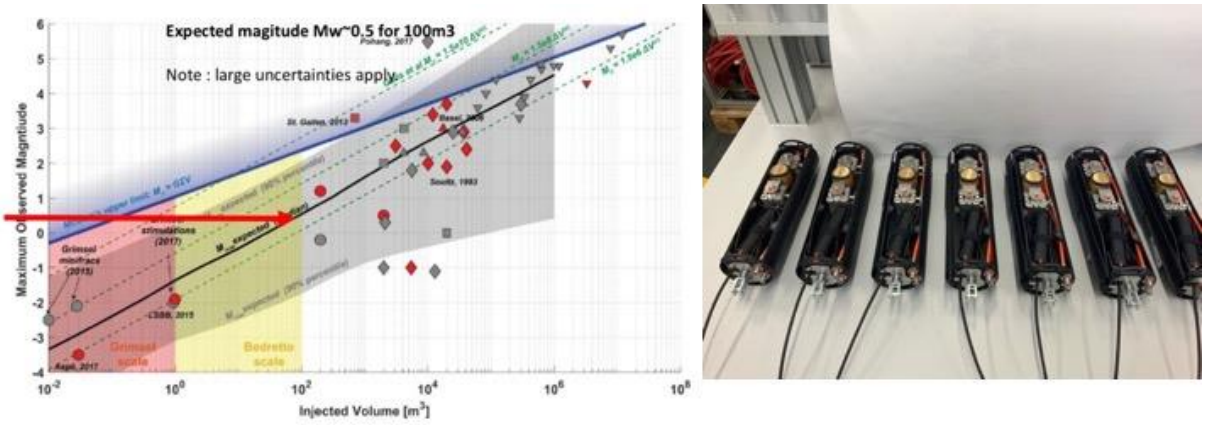

Figure 18. (Left) Seismicity estimation in Grimsel scale and Bedretto scale (Ma, 2019). (Right): Seismic monitoring network (Streamer 2.0) for seismic activity monitoring.

Seismicity is often associated with fluid injection at depth, including disposal of wastewater into deep formations, hydraulic fracturing of shale formations, and reservoir creation during the development of enhanced geothermal systems. It has been reported that the maximum seismic moment, induced by fluid injection, is limited to the volume of injected fluid times the modulus of the rock rigidity. According to this principle, given the expected injection fluid volume of a maximum of 100 m^3 in the BUL, we estimate a maximum event of 0.5 Mw (Figure 18). Note that large uncertainties apply to this estimation, due to the uncertainty of rock heterogeneity. To eliminate the theoretical uncertainties and support long-term seismic risk assessment in the BULGG, seismic monitoring is proposed for the BULGG. This monitoring network covers micro-seismic monitoring at scales of a hundred meters to about 10 km distance from the site, with typically earthquake magnitudes of 0.5 to 3.0 Mw. ETHZ also contributed to the design and construction of the sensors (Streamer 2.0) of the seismic monitoring network (Figure 18).

3.3 Collaboration between ETHZ and ESG

In WP 4: Environmental protection, ETHZ was planning to collaborate with GES and ESG on the effluents collection and measurements of the Rittershoffen site. A meeting between ETHZ (Dr. Xiangzhao Kong) and ESG (Dr. Nicolas Cuenot) took place at ETHZ on January 16, 2020. During that meeting, a general agreement has been made that ESG and ETHZ agreed to work together to carry out the planned tasks. On April 8, 2020, a detailed collaboration plan for Tasks 4.2 and 4.3 was proposed by ETHZ (Dr. Xiang-Zhao Kong) between ETHZ (Dr. Xiang-Zhao Kong) and ESG (Dr. Nicolas Cuenot):

(1) geochemical equilibrium calculations on the measured gas concentrations and species concentrations;
(2) investigation of the gas composition discrepancy between measurements of the effluents and the emitted gases at the venting valves;
(3) geochemical equilibrium calculations (mainly super-saturation of potential minerals) on the deposit scales at the heat exchangers;
(4) geochemical equilibrium calculations on scale inhibitors to control scaling.

To carry out this collaboration plan, ESG agreed to share with ETHZ the measurement data from the Rittershoffen site. ETHZ thus started preparing the data transfer agreement. However, from that time on, there has been no further response from ESG (possibly because of the COVID-19 pandemic), despite several (~5) contact attempts over several months following April 8, 2020, by Drs. Kong and Saar to contact ESG. In June 2021, ETH learned that Dr. Nicolas Cuenot was leaving ESG. Despite that ETHZ wanted to conduct the proposed tasks with ESG at the Rittershoffen site, the collaboration in WP 4 on Tasks 4.2 and 4.3 between ESG and ETHZ was unfortunately not possible to be carried out, given the unfortunate and difficult circumstances. In total, ETHZ has spent 49.2 personnel hours on WP4. The rest of the personnel hours of WP4 (about 944 hours) has been used to carry out the additional works in WP 2 and WP 3, as previously explained in paragraphs above.

4. Conclusions

ETH Zurich has worked on fracture analysis, stress analysis, injectivity test, measurements of deformation modulus and elasticity modulus, and borehole breakout analysis for several boreholes at BULGG, using various methods, including Acoustic Televiewer (ATV) and Optical Televiewer (OTV) investigation, mini-frac tests and dry (packer) reopening tests, step-rate injection tests, dilatometer tests, sleeve fracturing method, fracture compliance method, G-function, square root of time, bilinear pressure-decay, and jacking pressure analyses techniques. Various important parameters have been obtained, including BULGG in-situ stress, (rock matrix and fracture) injectivity, deformation modulus, elasticity modulus, pore fluid pressure, slip tendency, fracture density, fracture orientation, and etc. Various flow-through experiments of ETHZ yielded critical insights in the relationship between fracture transmissivity and the applied mechanical stress, thermal stress, and chemical stimulation. In particular, ETHZ has performed experiments of mud infiltration into fractures to examine the mud cake formation process. The shear-slip experiments yielded critical estimates on fracture combined rigidity, seismic moment magnitude, standard seismic moment, and maximum seismic moment. ETHZ also gave estimates on fluid injection-induced seismicity at BULGG.

5. References

X.-Z. Kong, J. Ma, M. Grimm Lima, and M.O. Saar. Experimentally exploring permeability evolution induced by THMC-coupled processes. 2019 ARMA-CUPB Geothermal International Conference.

X. Ma. Bedretto Underground Laboratory (BUL), Switzerland, and the planned in situ hydraulic stimulation experiments for EGS. 2019 ARMA-CUPB Geothermal International Conference.

K. Bröker. In-situ stress and rock mass characterization via mini-frac tests at the Bedretto Underground Laboratory. Master thesis. August, 2019.

K. Bröker, X. Ma, M.O. Saar, and the Bedretto Lab Team. In-situ stress and rock mass characterization via mini-frac tests at the Bedretto Underground Laboratory. 7th European Geothemal Workshop Karlsruhe, 9-10 October, 2019.

X. Ma, N Gholizadeh Doonechaly, M Hertrich, V Gischig, D Jordan. In situ stress characterization in the Bedretto Underground Laboratory: implications for induced slip of pre-existing fractures/faults. 3rd Schatzalp Workshop on Induced Seismicity 2019.

X. Ma, N. G. Doonechaly, M. Hertrich, V. Gischig, and G. Klee. Preliminary in situ stress and fracture characterization in the Bedretto Underground Laboratory, Swiss Alps: implications on hydraulic stimulation. ISRM 14th International Congress of Rock Mechanics Rock Mechanics for natural resources and infrastructure development Foz do Iguassu, Brazil, Sep 13-18, 2019, 2019.

Rutger van Limborgh, Borehole Indicators of In Situ Stress Field Heterogeneity at the Bedretto Underground Laboratory. Master thesis. August 2020, ETH Zurich.

X.-Z. Kong, M. Grimm Lima, X. Wang, J. Ma. (2021). Evolution of fracture permeability induced by THMC-coupled processes, InterPore 2021, Online.

Qing-Hua Wang, Laboratory Experiments on Mud Cake Formation in the Single Natural Fractures. Master thesis. September 2021, ETH Zurich.

Z. Li, X. Ma, X.-Z. Kong, M. O. Saar, D. Vogler. (2021). Permeability evolution during pressure-controlled shear slip in saw-cut and natural granite fractures. Submitted to Geomechanics for Energy and the Environment.

X.-Z. Kong, X. Wang, J. Ma, M. O. Saar. (2021). Shear and acidizing stimulation of carbonate-filled fractured granite. In preparation.

